Journal of
Earth Science & Climatic Change

Jabli et al., J Earth Sci Clim Change 2019, 10:1
DOI: 10.4172/2157-7617.1000506

Research Article Open Access

Physical - Mechanical Characterization of the Limestones of the Merfeg Formation (Campanian-Maastrichtian) in Central Tunisia and their Industrial Valorization

Ikram Jabli*, Tahar Aloui, Houda Khaled and Fredj Chaabani

Department of Geology, University of Tunis El-Manar, Tunis, Tunisia

Abstract

This paper investigates the suitability of the Campanian-Maastrichtian reef limestones from Merfeg Formation in Central Tunisia for a potential of use in the painting industry. Samples were milled to a specific surface area of approximately 3500 ± 250 cm^2/g. Physical and mechanical behavior, including (chemical-mineralogical composition, particle size distribution, optical performance, thermal behavior, density, Los Angeles abrasion tests and Micro-Deval and oil absorption) for raw material and the physical and mechanical behavior including (pH, viscosity, density and dry extract, visual glossiness wet film thickness and Wet abrasion resistance) for the paint films were carried these tests meet all standard requirements. The results show that the middle (second class) limestone of the Merfeg formation is marked by a high degree of purity, low levels of harmful oxides such as Fe_2O_3, MgO and SiO_2, brightness high (more than 86.5, 95.2 on average) with relatively low chromaticity (a^*<3.3, b^*<9.1), low oil consumption (18 ml/100 g of limestone on average), good grindability and acceptable abrasion range (10-17) and improved rheological properties. The calcium from the Merfeg formation appears to be suitable filler for the paint when mixed with water. On average, the formulated emulsion paint was composed of 58.8% calcium carbonate as filler, 28.9% water, 6% acrylic styrene, 4.5% TiO_2 as pigment and additives currents (1.8% in total). The formulated paint films meet all standard requirements, in that they have very good opacity, high luminescence (L^*=96.4), good pH buffering (close to 9), appearance and washability (wet abrasion resistance less than 5 µm). The performances of the films are similar to those based on the Barre de Ghoumrassene Member and El Garia Formation in Southeast and Northeast Tunisia respectively; however, they are slightly lower than the Abiod Formation (a lateral equivalent of Merfeg Formation) from the Feriana Hill in West-Central Tunisia and the Aşıgediği Formation in South Central Turkey. Henceforth, the studied carbonate, calcium might be valorized in paint industry, which are eco-friendly and easy to apply.

Keywords: Limestones; Merfeg formation; Raw material; Physico-chemical characterization; Valorization; Paint film

Introduction

Carbonate rocks are very important natural materials, which are used in a wide range of industrial and manufacturing applications depending on their physical and chemical properties [1]. In Tunisia, substantial reserves of limestones were deposited in carbonate platforms during Permian, Mesozoic and Tertiary intervals [2-4]. The Permian carbonates, outcrops in the eastern part of Jebel Tabaga of Medenian (South Tunisia, are predominately consisted of brown to cream dolomites, alternating with sandstone or calcareous levels [5]. The Jurassic deposits include the Barre de Ghoumrassene Member [3,6,7]. The most important are Cretaceous reserves include the Bouhedma Formation, [2,8] the Orbata Formation, the Zebbag Formation and equivalents [2,9]. Tertiary deposits are represented mainly by the limestones of El Garia Formation attributed to the Early Eocene [10,11] and Bou Dabbous Formation, most of these limestones are dolomitized or fractured and karstified, which limit their potential use for more value-added applications [12] (Figure 1).

White limestones are very limited and localized. The main most white outcrops belong to the Abiod Formation in Feriana Mountain and adjacent part of [3,13,14,15], due to their high degree of purity, whiteness, nature and ease of access, these carbonates are widely used in many industrial applications such as paper, white cement, painting and pharmaceutical products, [16,17]and water treatment [18]. In fact, these resources are over exploited and other materials should be considered. The Merfeg Formation, which is a lateral equivalent of the Abiod Formation) [19-21], and the nummulitic limestones of the El Garia Formation [10,11] (Figure 2). However, those of the Merfeg Formation have not received enough attention and research priority that they deserve. The suitability of use for any given application depends in particular, on mean particle size and distribution, color, chemical composition, and mineral purity of the material [22,23]. The production of paint is the result of a mixture of heterogeneous materials including pigments, fillers, acrylic resins mixed with water and other adjuvants. In the paint industry, the ground calcium carbonate is employed throughout the range of water- and solvent-based coatings for both interior and exterior applications [24]. The present work tries to evaluate the relevance of the white carbonate of the Merfeg Formation in the Jebel El-Kébar for the first time for the paint industry. The studied carbonate calcium might be valorized in paints, interior applications which are eco-friendly and easy to apply.

Geological settings

At the end of the Cretaceous, a carbonate platform is widespread throughout Tunisia. However, during this period, Central Tunisia

***Corresponding author:** Ikram Jabli, Laboratory of Mineral Resources and Environment, Department of Geology. Faculty of Mathematical, Physical and Natural Sciences of Tunis, University of Tunis El-Manar, 2092 - Tunis, Tunisia, Tel: +223 71 99 02 82; E-mail: mjabligeologie@gmail.com

Received December 09, 2018; **Accepted** January 10, 2019; **Published** January 18, 2019

Citation: Jabli I, Aloui T, Khaled H, Chaabani F (2019) Physical - Mechanical Characterization of the Limestones of the Merfeg Formation (Campanian-Maastrichtian) in Central Tunisia and their Industrial Valorization. J Earth Sci Clim Change 10: 506. doi: 10.4172/2157-7617.1000506

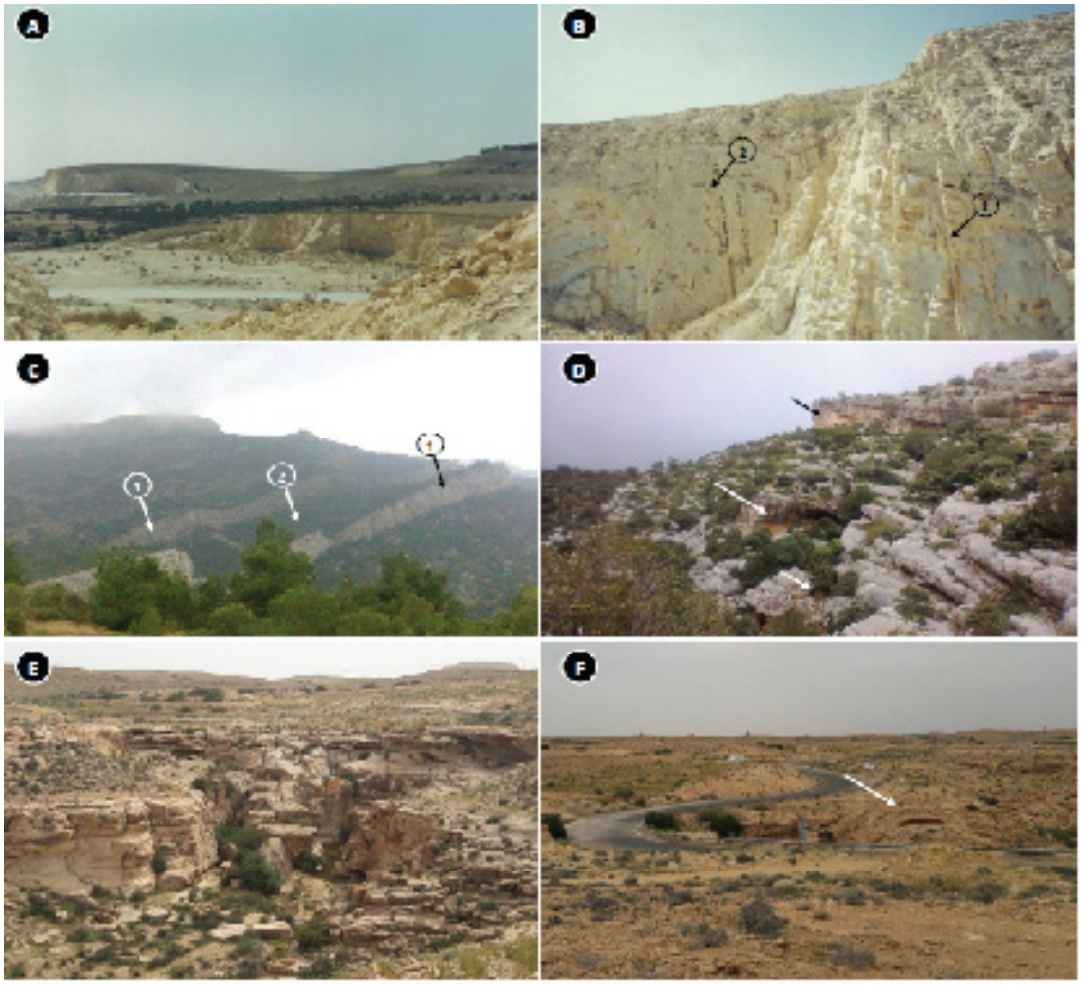

Figure 1: Main outcrop features of the Bou Dabbous and Serdj Formations and the Barre de Ghoumrassene Member. A: Panoramic view of the Bou Dabbous Formation (Ypresian) near Bizerte town in North Tunisia. B: Closer view of (A) chowing near vertical layers of white limestone (1), and folded layers (2). C: Panoramic view of the Serdj Formation at Serdj Hill in Central Tunisia. Alternations of gray to cream reef limestone (1), and clays (2). D: Upper term of the Serdj Formation displaying karstification and small grottos (arrows). E: Outcrops of the limestone of the Barre de Ghoumrassene Member in Southeast Tunisia. F: Bioherm constructions at the top of the Barre de Ghoumrassene (arrow).

experienced positive movements that led to the uprising of the shoals called the "Central Tunisia Platform" [2].

This new paleogeographic configuration is expressed by the presence of intracratonic basin of Gafsa in the south and the Tunisian furrow to the north. Both have played the role of trap stopping the detritic sediments coming from the Saharan platform in the South and the edge of the Central Tunisia platform to the North. Sheltered from any detrital sedimentation, a particular environment has developed in central Tunisia characterized by a shallow depth and a permanent agitation of the water. Reef constructions have been able to develop in some localities in central Tunisia and particularly in Jebel Sarraguia and Jebel el Kébar level [25-27]. This particular arrangement has made the locality of Jebel el Kébar a well-illuminated vane environment favorable to the development of rudists who could reach very important sizes. These organisms with carbonate shells are at the origin of the white limestone which is the object of our study. However, the Merfeg Formation, which is a lateral equivalent of the Abiod Formation [19,21,25], belonging to the lowest division of the Campanian-Maastrichtian. Correlated to the Abiod Formation is one of the main deposits of extra-white limestones [12,16].

The Merfeg Formation is generally composed of three massive carbonate members containing rudists and interbedded with few marly limestone beds [19,28,29]. The first member corresponds to a massive limestone with some marly and dolomitic intercalations. The second and third members show a constant thickness and they are constituted by centimetric to metric limestones beds. The biogenic assemblage is mainly composed of rudists and polyps. The limestones of Merfeg Formation have overlain the marly limestones and the clays of Aleg Formation (Coniacian-Santonian). The Merfeg Formation (upper Campanian) crops out around the southwestern periclinal termination of Jebel El Kébar constitutes the main reliefs of Rouss al Kebar, Jebel Al Frayou and Jebel el Merfeg [19]. The studied area is located in the south-west of Jebel El Kébar constitutes a large NE-SW trending anticline about 20 km long and 6 km wide, emerging in the plain of Sidi Bouzid, about 10 km west of the N-S axis, the eastern of Jebel Merfeg and Khanguet Réhouis [19,30,31] (Figure 3).

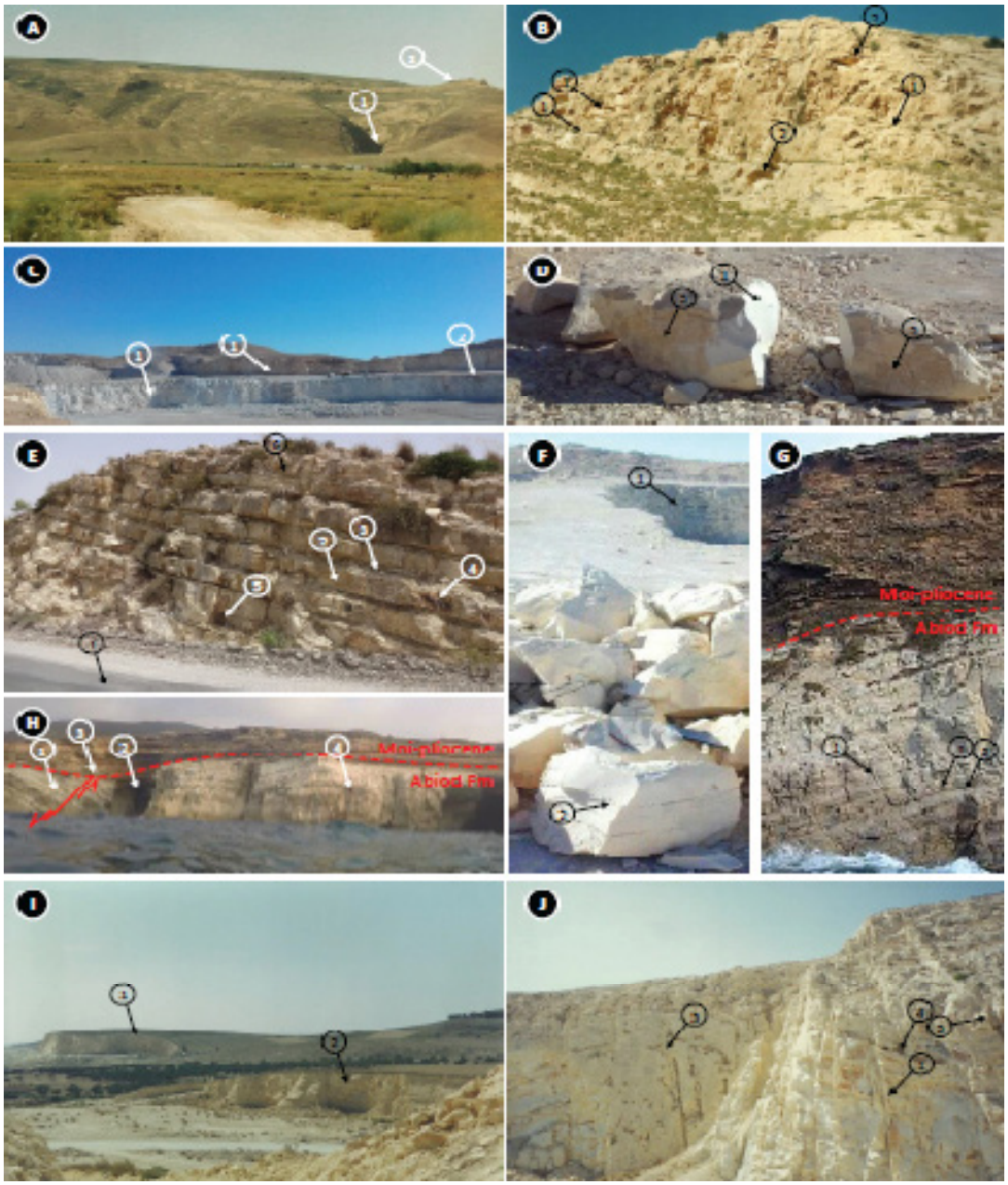

Figure 2: Outcrops of main equivalents white limestone in Tunisia. A: Overview of the reef limestone (Abiod Formation) of the Sarraguia Hill in West-central Tunisia. B: Closer view of the upper term of the Abiod Formation at Sarraguia Hill showing the karstification near bedding planes (1), and the pseudo nodulation of the limestone (2). C: Outcrops of the Abiod Formation at a quarry for gray Portland cement at the Rouissat Hill (Central Tunisia). D: Closer view of the (C) showing the high whiteness of a hard limestone at fresh plane (1), and red hue due to water circulation on discontinuities between beds (2). E: Upper term of the Abiod Formation at the Mansour Hill (North Tunisia), showing intercalations of soft marls (1), rare nodules of iron (2), mineralization (3), and abundant fracturing of strata (4). F: Closer view of (C) showing small karsts (1), and well exposed stylolite marks. G: upper part of the Abiod Formation at Methline beach in extreme North Tunisia, with abundant fracturing strata (1), and marl interbeds (2). H: Panoramic view of (G) showing abundant and thick interbeds of marls and clay (1), grottos (2), faults (3), and karsts (4).

Data and Methods

Collection and conditioning of raw samples

Fifteen representative samples were collected (Figure 4). The sampling procedure depended on lithology and thickness of beds. If the later was less than 5 m, one sample was taken from the middle. If the thickness exceeded this limit, one sample was taken from the middle. If the thickness exceeded this limit, one sample was taken every 5 m. The raw samples were dried in an oven at a temperature of about 105°C for 1 h and turned into fine powder using HERZOG High Speed Mill (HSM).

Physical behavior of the raw material

Chemical composition: The main chemical compositions on

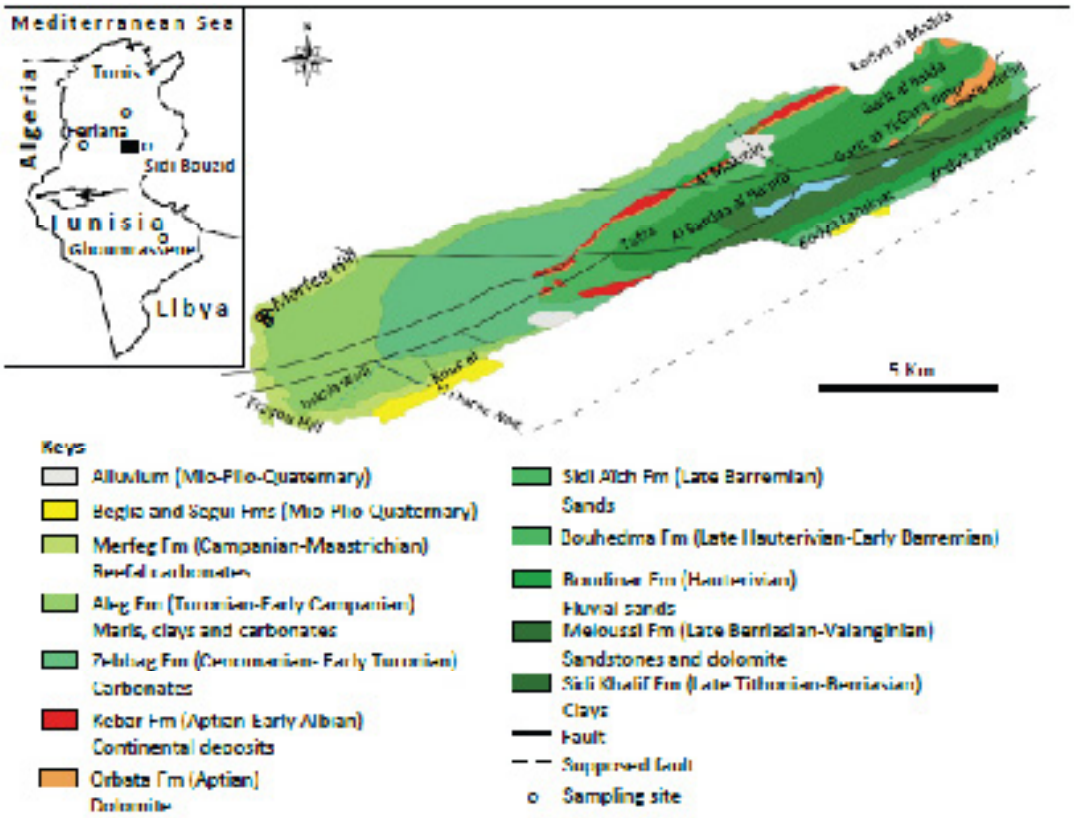

Figure 3: Geological map of the El Kebar Hill, chowing the location of the sampling site (Modified after (Khessibi [18], Ouali et al. [29] and Jaballah and Negra [30]).

major elements as alumina oxide (Al_2O_3), calcium oxide (CaO), ferric oxide (Fe_2O_3), magnesium oxide (MgO), titan dioxide (TiO_2), and silicon dioxide (SiO_2) were determined by X-ray Fluorescence method (XRF) on a Philips PW 1606 spectrometer with automated sample feed, reverse potential end window with Rhodium anode and operated at 50 kV, 40 mA. Beads were prepared by fusing mixtures of 0.7g of the powder sample with 6 g of lithium tetraborate (LiB_4O_7) [32,33]. These steps taken in preparation of the sample led to a more homogeneous material and, consequently, had the advantage of obtaining a more accurate XRF analysis. The contents of potassium oxide (K_2O) and sodium oxide (Na_2O) were analyzed by Atomic Absorption Spectrometry (AAS).

Mineral composition and infrared spectra: The mineralogical composition was determined by using X-ray Diffraction (XRD) and Infra-Red Spectra (IFS) techniques. The XRD analysis was carried out by using a Philips PANalytical X'Pert PRO X-ray Diffractometer with an automatic divergence slit, a spinner, an X'celator, and CuKa radiation at a scan speed of 0.01° 2θ/s. The acceleration power applied was 40 kV, with a current of 40 mA. The difference between the experimental and the theoretical peaks of Si (111) was within 2θ=0.002° and the resulting diffractograms were interpreted by X'pert HighScore plus software. Infrared spectra were obtained using a JASCO FT-IR-420 spectrophotometer. The pressed-discs, we prepared using 1 mg of the selected samples which was diluted with 200 mg KBr. Transmittance spectra were recorded in the MIR region 4000 to 400 cm^{-1}. The $CaCO_3$ content was estimated by using the Bernard Calcimeter Method.

Optical performance of raw materials: The whiteness index is an important measures of the color of materials for industrial applications such as white cement, paper and paint industries. First, 10 g of the material was placed in a pellet and then stacked by using an Elrepho 450X Spectrophotometer according to the International Commission on Illumination standard (CIE) in 1986) [34]. Results were expressed in the $L^*a^*b^*$color system, where L^* (white-black reading) indicates the lightness or luminescence of the sample, a^* indicates the tendency towards the red green color and b^*, however, expresses the tendency towards blue or yellow tint. The CIE L^* a^* b^* color space was chosen since it is widely used in paint and coating industry

Particle size distribution: The grain-size distribution of the ground particles was out using a Laser Particle Sizer model Analyzer 22/NanoTec (FRITSCH GmbH, Germany), with a measuring range of 0.01-2100 µm. The particle size distribution data include mean and median sizes of the samples tested, their 45-µm percent passing value, size, and spread factors (n, X_0) of the Rosin– Rammler distribution and Blaine specific surface area values. The size and the shape of the ground particles play a key role in the production processes the performance of the end product in particular resistance to abrasion, UV radiation, weathering forces and appearance of the surface film [35].

Thermal behavior: Thermal Gravimetric Analysis (TGA) and Differential Thermal Analysis (DTA) were performed with a SETRAM type 124 TG/DTA instrument using aluminium as inert reference material. Temperature was increased from room temperature to 1100°C at the regular increment of 10°C/min in air atmosphere. The

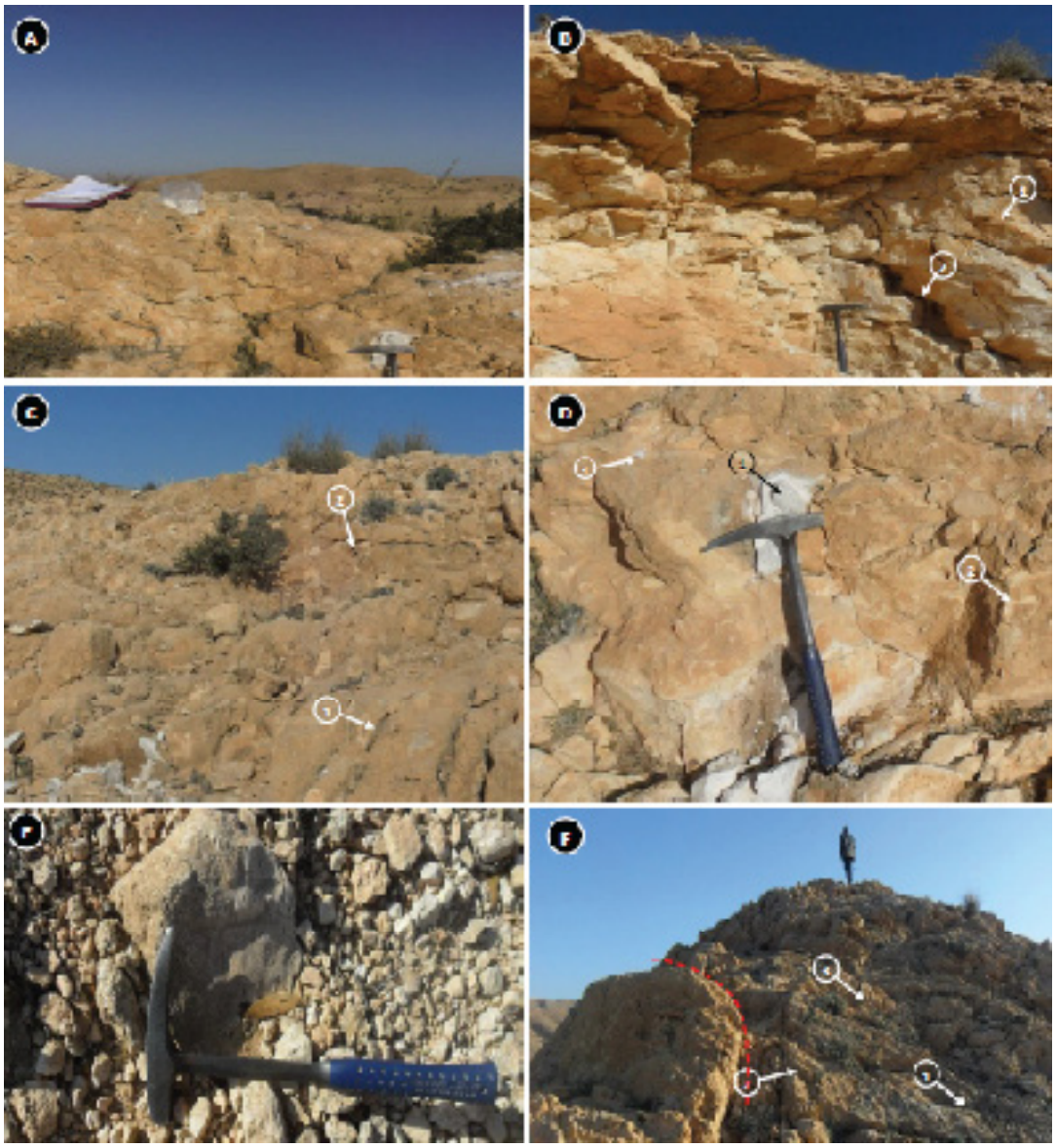

Figure 4: Outcrops of the Merfeg Formation. A: Overview of the limestone showing the upper term of the Merfeg Formation. B: Closer view of (A). C: Upper term of the Merfeg Formation showing indices of karstification (1) and fracturing (2). D: closer view of (A), showing the whiteness of limestone (1) and rare debris of rudists (2). E: Coral. F: Karstification in bedding planes (1), fracturing (2) and faulting (3) at the upper most term of the Merfeg Formation.

thermal behavior allowing to detect volatiles and organic matter and to evaluate how materials exhibit either mass loss or gain during the decomposition and oxidation process.

Mechanical behavior of the raw material: Several tests were checked for the mechanical behavior of the raw material including density, abrasion test by Los Angeles and Micro-Deval tests and oil absorption, these tests meet all standard requirements.

Density: This test is performed using 100 ml pycnometer at room constant temperature and pressure. A dry, weighed glass pycnometer (Mp), was filled with distilled water, and then weighed (Mp+w), giving the weight of water (Mw=Mp+w - Mp). The ground sample was added to the pycnometer (Mp), which is then weighed (Mp+GS). The weight of the powder is MGS= Mp+GS - Mp. The pycnometer is then filled with distilled water, in which the sample was completely insoluble. The weight of water and powder is Mw+GS, and thence the density of the sample dGS was calculated as follows: dGS=MGS/(Mw - Mw+GS) [7]. The test was done at room temperature and pressure as suggested by the (ASTM D854 norm: ASTM 2014 a) [36].

Resistance to fragmentation: The Los Angeles (LA) test is used to measure the resistance to fragmentation of aggregates caused by falling the steel balls in a rotating cylinder under standard conditions of the ASTM D 6928 norm (ASTM, 2017 a) [37]. It consists to calculate the weight of aggregates less than 1.6 mm produced by fragmentation. LA=100*m/M, where M=5 Kg of sample and m=the weight of aggregates coarser than 1.6 mm.

Wear resistance: The Micro-Deval test in the presence of water

(MDE) is used to determinate the attrition due to aggregates under an abrasive charge. It consists to measure the wear produced on a cylinder under standard conditions by friction between the aggregates and the abrasive charge. The Micro-Deval was computed as MD=100*m/M, where M=500 g of raw materials and m=the weight of aggregates coarser than 1.6 mm. the limestone aggregates was done using Micro-Deval testing in accordance with ASTM D 6928 norm (ASTM 2017a) [37].

Oil number: The oil number (oil absorption) of a given filler or pigment is the number of milliliters of linseed oil used for 100 g of dry pigment to produce a smooth and cohesive paste. The value of the oil intake is expressed on the basis of volume/mass or mass/mass. The oil consumption was used to give an indication of the effect of different fillers on the flow properties and to calculate the pigment loading limits [35]. The oil adsorption was done according to the ASTM D 281 norm (ASTM 2016) [38]. Oil intake is generally required to be compared with the value determined at the same time on an approved product sample.

Paint formulation and preparation: The formulation of paints involves the use of minerals of various natures and with adequate proportions. Paint is characterized by their hue, opacity, shiny or satin appearance. In general, paint emulsion consists of pigments, fillers, binders, diluents and various [39]. During formulation, the nature of additive and its proportion were optimized according to their compatibility in particular with the used binder (styrene acrylic binder) [40]. The function and the proportion of each component are reported in Table 1.

The pigment gives to the paint film color and opacity. The most pigment used is the TiO_2 because it is characterized by their high optical, rheological and mechanical performances [41]. The calcium carbonate filler is used to reduce the cost of paint. Very fine particle size silicates, as kaolins and ultrafine talcs, can enhance coating performance and provide very favorable economics by effectively separating the individual pigment particles and optimizing the opacity [42]. The binder is the major component of painting. It helps to the drying processes and forms the paint film. Solvent, however, gives the paint its correct consistency to make it easier for application. The additives were added to the emulsion in small quantities to give new performance to the film as anti-fungicidal agents, driers, pH adjuster, etc [35]. The major objective was to formulate white wall paint for interior use. Interior paints are mainly concerned with aesthetic characteristics such as color, gloss, washability and adhesion properties, rather than protection, which are relatively easy to apply [42]. The use of water borne paint is due to its increased demand, odorless and environmentally-friendly production, application and conservation methods when compared to the solvent based paints [7].

The paint formulation starts with the mixture of 70% by weight of ground carbonate and 30% of water, resin and pigment to form a high concentrated millbase (Table 1). To emphasize the load a carbonate to water ratio of 2/3 was used. The homogenization and the consistency of the mixture were achieved by means of a magnetic stirrer at 1000 rpm for 4 hours using a 12 mm ceramic ball mill. Coarser calcite particles were screened using a 63 µm seizes. After that, various additives and eventually binder were added in proportioned fractions and the emulsions were homogenized using the same dispositive for five minutes to complete the preparation.

Physical and mechanical properties of paints

pH measurements: The pH measurement is the measure of the acidity or alkalinity of a solution. The pH value was measured at room temperature using a pH meter. The pH electrode was calibrated against the buffer solution with a fresh calibration solution of pH 7.

Materials	Quantity (%)
HEC thickening agent	0.26
Anti-bacterial agent	0.26
Dispersion agent	0.006
Wetting agent	0.1
Anti-foam agent (Defoamer)	0.2
Filler: limestone of Merfeg	58.8
Pigment (TiO_2)	4.5
Water	28.9
PU: Thickening agent	0.1
Binder: Emulsion (styrene acrylic)	6
pH Stabilizer	0.02
Coalescing Agent	0.6
Blistering agent	0.004
Bioacide	0.25
Total	100
HEC: Hydroxyethyl Cellulose; PU: Polyurethane	

Table 1: Paint recipe.

Viscosity of the emulsion: Viscosity is the measure of the resistance of paint to deformation under constant shear stress [35]. It was made using a Brookfield viscometer in accordance with ASTM D562-10 (ASTM 2014b) [43] norm standard for painting, varnishes, glues, pastes and inks. The rotation of the spine was maintained at 200 rpm at a constant rate for 100 seconds and at a constant temperature of 25°C. The results were reported in Krebs unit (KU).

Density and dry extract of the emulsion: Density corresponds to the ratio between the mass of a given volume of material and the mass of the same volume of water or air. The dry extract (ES) is the determination of the density of the non-volatile ingredients (pigment and binder) of a paint and varnish. It is determined by passing through an oven whose temperature of 105°C, for 1 hour, expressed as a percentage in accordance with ISO 3251[44] norm standard for painting.

Physical and mechanical properties of the paint films

Visual glossiness: Gloss is a visual perception that occurs when viewing surfaces. The perception of brilliance is all the more marked as the light is reflected express in%. Gloss is measured by quantifying the reflectance of a known amount of light from a painted film surface. It was measured at dualgloss 20/60° following the ASTM D523 norm (ASTM 2008) [45].

Wet film thickness: Wet film thickness is the measured thickness of any applied wet paint that is liquid-based. It was carried out on a rigid substrate in compliance with the requirements of the ASTM D1212 norm (ASTM 2013[46]). The measures of wet film thickness should be on a wet film before a significant evaporation of the solvent occurs. The measurement of wet film thickness provides an early appreciation about the coating application process and the spreading rate of paints [35].

Dry through time: For testing the degree of through drying of a coating. A test plunger faced with nylon fabric and loaded with a defined weight is lowered onto the test surface for a period of 10 s, the film was not distorted or detached when the thumb was applied to it in a specified manner and then turned through 90°. The test was carried out at ambient temperature on a clean glass substrate and under no direct sunlight.

Wet abrasion resistance: The resistance to wet abrasion evaluates the resistance of a paint film to repeated washings [47]. This resistance is determined according to ISO 11998 [48]. The test coating is applied to a specimen using a film applicator set to the appropriate thickness. The sample is subjected to the action of a foam wiper performing a movement back and forth in the presence of water. After drying the 28-day film at 23°C (± 2°C) and 50% (± 5%) relative humidity, the painted specimen is weighed and then subjected to 200 wet rubbing cycles in a test machine. friction. The film was then washed, dried and weighed again to determine its mass loss from the average film thickness loss. It is by comparing the average thickness loss of the film that the class of friction resistance can be evaluated.

Data processing: To identify the relationships between chemical and optical variables and to determine which of them contribute most to the variation in the data set, a multivariate ordination technique, such as Principal Component Analysis (PCA). The principal component analysis described here is carried out without axis rotation and structured in 11 variables, which comprise eight chemical parameters (Al_2O_3, CaO, Fe_2O_3, K_2O, Na_2O, MgO, SiO_2 and TiO_2) and three optical stimulus (L^*, a^*, and b^*) and the Agglomerative Hierarchic Clustering (AHC) techniques were performed using XLStat-pro software (Addinsoft 1995-2017, Ver 19.4). All original chemical and optical variables were assumed to have an equal importance in their influence on material quality.

Results and Discussion

Mineral and chemical properties of raw materials

The mineral cortege of limestone from the Merfeg Formation is composed quasi-exclusively of calcite as can be deduced by XRD (3.034 Å, 3.86 Å and 3.84 Å) (Figure 5). Infrared spectra patterns (1434.07/cm and 870, 31/cm) (Figure 6).

The purity of the material estimated by Bernard calcimeter method ranges from 96 to 99% $CaCO_3$ with an average of 98% $CaCO_3$. Higher values were observed at the top and the middle part of the lithostratigraphic column. These results are in good agreement with chemical results that evaluate the percentage of calcite based on CaO levels to 98.5% to 99.2%, which confirm the high to very high purity of the limestone from the Merfeg Formation.

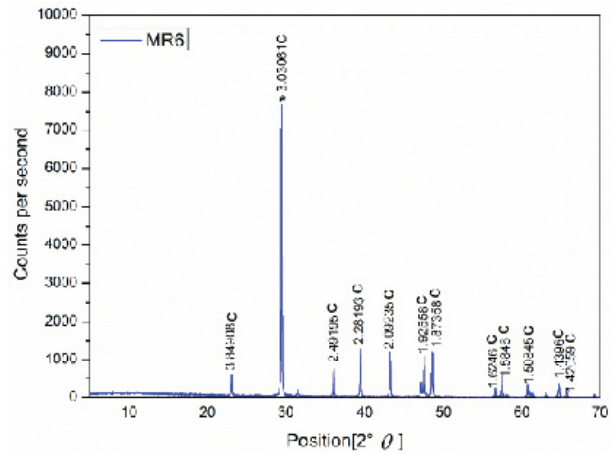

Figure 5: Pattern of X-ray powder diffraction, showing the mineral composition of the limestone from the Merfeg Formation (MR6 sample).

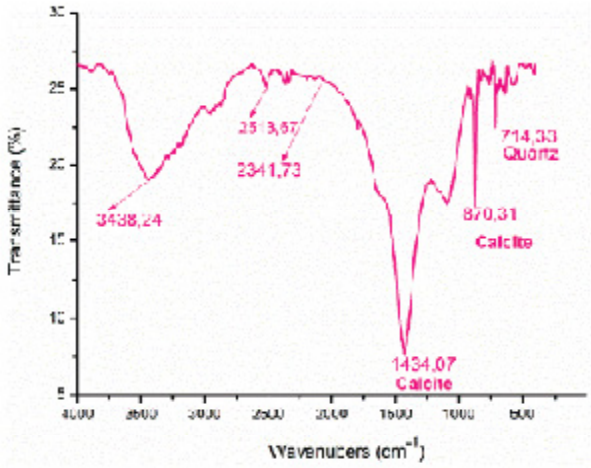

Figure 6: Infra-red spectra of limestone from the merfeg formation (MR6 sample).

The amounts acid insoluble and harmful oxides as MgO and Fe_2O_3, are relatively low for all samples (less than 0.1% for acid insoluble and 5.5% and 1% for MgO and Fe_2O_3 respectively), (Table 2) the amounts of SiO_2 and Al_2O_3 are generally low without exceeding 3.1% and 1% respectively. These elements can be attributed to clay fraction.

The alkaline oxides are extremely low without exceeding 0.05 and 0.3% respectively for Na_2O and K_2O. The Pearson correlations (Table 3), show strong link between major part of considered parameters in particular for CaO and LOI (r=0.988), L^* and CaO (r=0.984). To reduce the dimensionality of the dataset and to determine the correlation between the different variables, a PCA has been implemented. The variability explained by the two first factors is relatively high (91.4%). This projection ensures that the map based on F1 and F2 axis only has a good projection of the initial data (Figure 7). The strong and positive correlation between CaO and LOI (r= 0.988) suggests that LOI is exclusively due to the decarbonation of calcite. The strong and positive correlation between lightness (L^*) and CaO can be explained by the presence of white mineral in particular calcite. The positive and strong correlation between Fe_2O_3, Al_2O_3, SiO_2, MgO and K_2O+Na_2O ($r \leq 0.504$) can be attributed to clay minerals as illite ($(K, H_3O)(Al, Mg, Fe)_2(Si, Al)4O_{10}[(OH)_2,(H_2O)]$, kaolinite $Al_2Si_2O_5(OH)_4$ and residual materials of alteration, which contribute to the decrease of the overall whiteness of the materials which can be deduced from the strong negative correlation between L^* these parameters ($r \leq -0.85$). The TiO_2 seems to be not correlated with any of optic readings L^*, a^* and b^* which indicates that it contributes weekly in the chromaticity and luminescence of analyzed samples.

The reading of brightness increases with increasing light mineral content in the form of calcite and decreases as the level of dark minerals, especially iron oxides and clay minerals, increases. These seem to be the main factor responsible for the color changes of the limestones. The red stimulus (a^*) is greater than zero for all the samples considered, which assumes that iron oxide is the most common impurity that causes variations of white over manganese and titanium oxides. Similarly, the yellow stimulus (b^*) is superior to a red stimulus (a^*), suggesting, theoretically, a light-yellow appearance. Visually, the rock has a clear reddish hematite-like hue, which masks the yellow color of goethite (Fe_2O_3 and FeO(OH) respectively [12]. The squared cosines of the

Variables	CaO	MgO	SiO_2	Al_2O_3	Fe_2O_3	TiO_2	Na_2O+K_2O	%LOI	L*	a*	b*
CaO	**1**										
MgO	**-0.974**	**1**									
SiO_2	**-0.957**	**0.912**	**1**								
Al_2O_3	**-0.925**	**0.967**	**0.86**	**1**							
Fe_2O_3	**-0.848**	**0.845**	**0.807**	**0.835**	**1**						
TiO_2	-0.484	0.393	0.504	0.429	0.501	**1**					
Na_2O+K_2O	**-0.739**	**0.773**	**0.785**	**0.805**	0.505	0.431	**1**				
%LOI	**0.988**	**-0.985**	**-0.953**	**-0.944**	**-0.82**	-0.483	**-0.82**	**1**			
L*	**0.984**	**-0.957**	**-0.932**	**-0.916**	**-0.857**	-0.481	**-0.698**	**0.963**	**1**		
a*	**-0.986**	**0.967**	**0.958**	**0.928**	**0.815**	0.458	**0.779**	**-0.983**	**-0.984**	**1**	
b*	**-0.976**	**0.948**	**0.913**	**0.906**	**0.851**	0.479	**0.68**	**-0.952**	**-0.997**	**0.971**	**1**
Values in bold are different from 0 with a significance level alpha=0.05											

Table 2: Correlation matrix of Pearson (*n*) of chemical and optical parameters.

Variables	F1	F2	F3	F4	F5	F6	F7	F8	F9
CaO	**0.978**	0.002	0.003	0.009	0	0.004	0	0.001	0.002
MgO	**0.956**	0.023	0	0.004	0.004	0.009	0.001	0	0.002
SiO_2	**0.918**	0	0.002	0.02	0.055	0	0.004	0.001	0
Al_2O_3	**0.91**	0.01	0.003	0.051	0.017	0	0.009	0	0
Fe_2O_3	**0.752**	0.006	0.148	0.07	0.022	0.002	0.001	0	0
TiO_2	0.282	**0.714**	0.001	0	0.003	0	0	0	0
Na_2O+K_2O	**0.634**	0	0.345	0.012	0.003	0.005	0.002	0	0
%LOI	**0.982**	0.003	0.004	0.001	0	0.008	0.002	0	0
L*	**0.961**	0.002	0.015	0.012	0.004	0.005	0	0	0
a*	**0.973**	0.007	0	0.012	0	0	0.001	0.006	0
b*	**0.942**	0.002	0.02	0.014	0.01	0.009	0.001	0.001	0
Values in bold correspond for each variable to the factor for which the squared cosine is the largest									

Table 3: Contribution of variables for the first 9 factors.

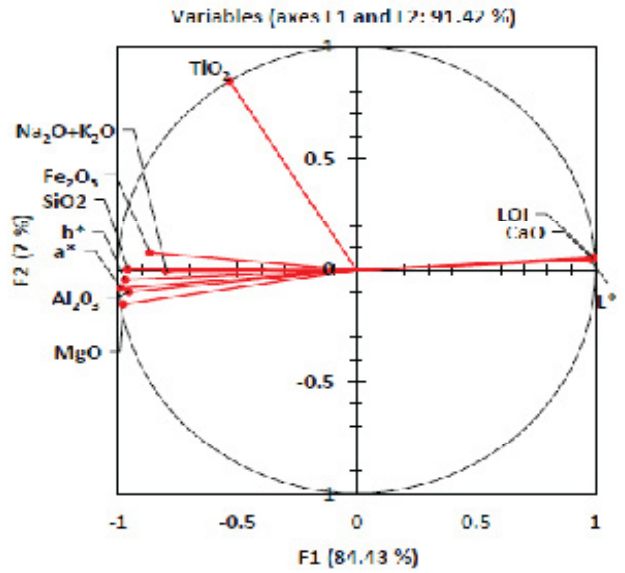

Figure 7: Correlation circle of variables based on F1 and F2 factors.

variables (Table 3), indicate that except for TiO_2, which is associated with F2 factor (cos^2=0.714), the rest has variables are clearly linked to the first factor ($cos^2 \geq 0.634$ for Na_2O+K_2O).

The Agglomerative Hierarchical Clustering (AHC) subdivided the limestones of the Merfeg Formation into three main groups, which differ essentially in their whiteness. The first group including white limestone (MR1-MR5), the second one is composed of relatively very white limestone, (MR6-MR11 and MR13). The last group is constituted of darker and more colorful limestone, which includes MR12 MR14 and MR15 samples. The barycenters of these groups are MR3, MR6 and MR15 respectively (Figure 8).

Physical and mechanical properties of raw materials

Density, resistance to fragmentation and wearing: The density of limestone ranges from 2.64 to 2.7 with an average of 2.68. The wet Micro Deval and Los Angeles values experienced a relatively wide range of variation and were in the ranges of 10-17% and 15-25% respectively for all tested samples. These differences can be attributed to the vertical and lateral variations in lithology within the Merfeg Formation. Hence, an adequate conciliation between the mechanical resistance of raw materials and the paint film should be considered during exploitation. Indeed, grinding properties of raw materials are an important process in the paint industry [7]. The reduction of calcite particles size is very expensive, and the energy needs as well as the cost per ton of charge [49].

Thermal behavior: Through the thermogravimetric analysis depicted in Figure 9, all tested samples exhibited a slight loss in weight by about 1% at 100°C due to the evaporation of free water as humidity or adsorption on the surface of the sample. When temperature reached 880°C, samples showed a sharp endothermic peak with a loss of about 55% of the weight due to decarbonation of the calcite.

Grain size distribution: Particle size distribution plays a key role in production processes of paint and coating in term of calcium absorption and retention as well as in the quality control of the end-product. The distribution of ground calcite particles is depicted in the semi-logarithmic curve of Figure 10. The average equivalent spherical diameter (D50), was between 2 and 10 µm (common interval is 10-18 µm) [35]. The 3rd and 97th percentile as indicators of finer and coarser

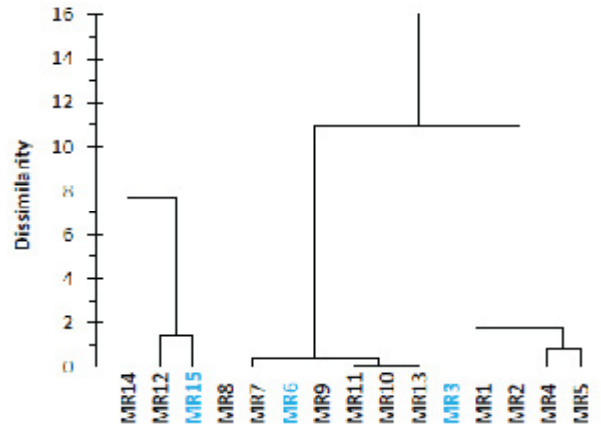

Figure 8: Dendrogram of the Agglomerative Hierarchical Clustering (AHC), showing three main classes of limestone and their barycenters (MR3, MR6 and MR15).

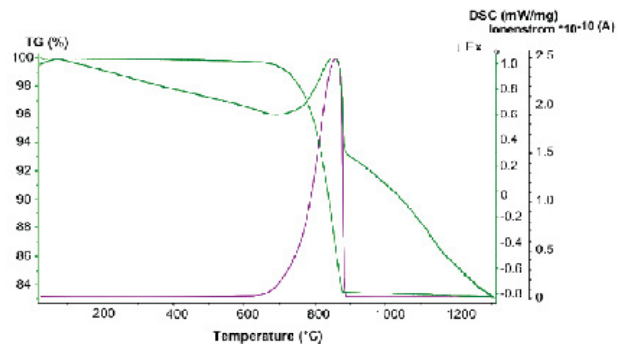

Figure 9: Thermal behavior of limestone from the Merfeg Formation (MR6 sample), investigated by Differential Scanning Calorimetry (DSC) and Thermo-Gravimetric Analysis (TGA).

particles were in the ranges 0.59-0.63 µm and 10.4-36.2 µm respectively. All these parameters are consistent with the requirements for paint and coating [35]. Likewise, the uniformity coefficient Cu=D60/D10 ranged from 3.75 to 5.625). However, the curvature coefficient $Cc=D30^2/(D60.D10)$ of calcite aggregates varied between 0.576 and 4.44. This indicates that the distribution was irregular in time and can be classified as well ranked with wide changes in grain size (Cu > 6 and 1 <Cc < 4) to poor (Cu ≤ 6). However, based on the mean values of the uniformity and curvature coefficients, the distribution can be considered as misclassified [7]. However, the decreasing in the theoretical mean diameter (Q50) contributes to scattering light by altering the spatial distribution of the pigments in the dry film.

Optical performance: The luminescence reading (L^*) of tested limestones was high and ranged from 83.66 to 94.58 (Figure 11). The hue of the samples was dull and overall showed a slight tendency towards the pink -red color (a^*=1-(1.6)-5.15 and b^*=4.6-(5.9)-11.2). The value of clarity L^* is more important for the median part of Merfeg Formation and it decreases from above and below (weathering and dolomites), the limestones typically become darker and reddish to yellowish in color.

To investigate the color changes of the limestone the iron oxides profil appear to be the primary factor responsible for color changes of the limestone indeed (Figure 12), the red reading (a^*) is higher than zero for all samples, which confirms that the other types of oxides have a secondary effect on the whiteness variation when compared to the iron [7]. On the other hand, the yellow reading (b^*) is characteristically higher than a^*, which suggests, theoretically, a light-yellow hue. Visually, the limestone has light pink hue due to hematite (Fe_2O_3), which masks the yellow color from goethite (FeO(OH).

Oil number: The oil absorption values are between 18 to 20 ml/100 g of limestone. This oil absorption is good because it requires fewer vehicles to bind, which leaves more vehicle available to bind to the substrate. The more oil absorbs matter, the less it is better. The difference in the number of oils can be attributed to the method itself, which is highly dependent on the operator [35].

The low oil number provides information on the shape, size and surface area of fine, medium and coarse calcite particles. Higher oil numbers of calcite are indicative of very fine calcite particles and regularly form with a higher specific surface area and therefore more binder (resin) is needed to bind them. However, the very low oil numbers (less than 15 ml/100 g calcite) indicate very coarse irregularly shaped calcite particles [23]. These results confirm an adequate grinding of limestones.

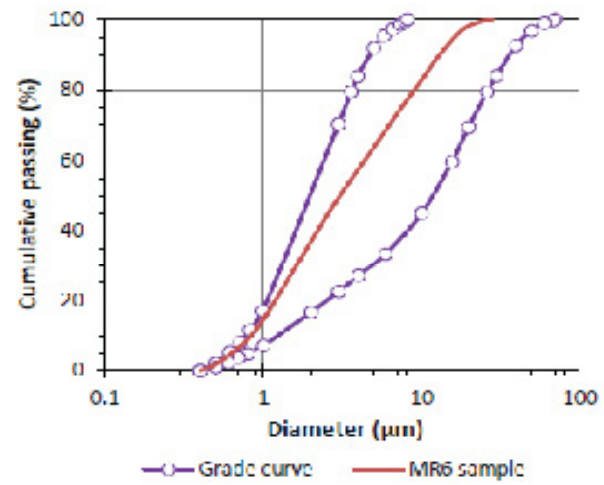

Figure 10: Grade curve of calcite aggregates from the Merfeg formation and particle size distribution of MR6 sample.

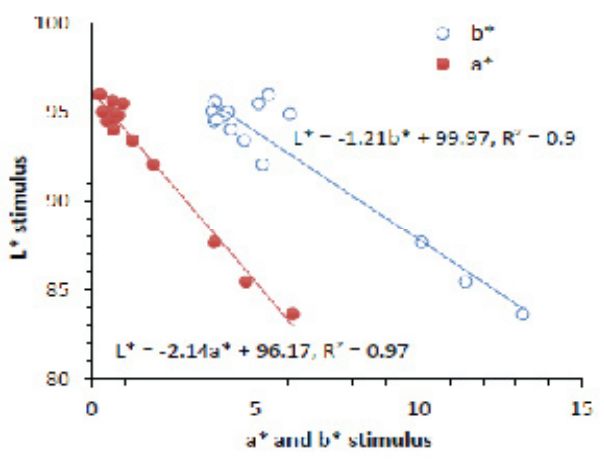

Figure 11: Variations of luminescence (L^*) as function of red-green reading (a^*) and yellow-blue reading (b^*) of carbonates from the Merfeg formation.

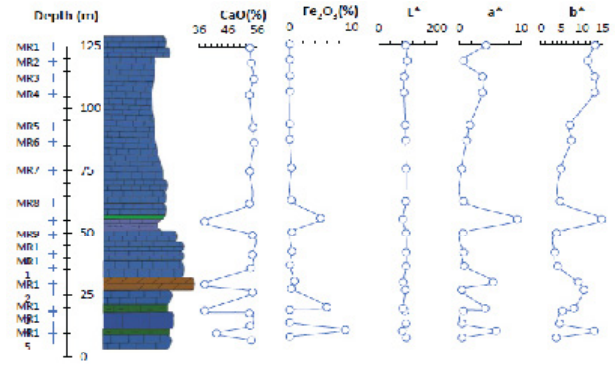

Figure 12: Vertical variations of CaO, Fe_2O_3 and a*, b* and L* stimulus of the Merfeg formation.

Physical and mechanical properties of paints

The main characteristics of formulated emulsions include pH, viscosity, density and dry extract.

pH and viscosity: pH and viscosity are the main characteristics for paints and varnishes, a decrease in pH can affect largely the end product performance and conformance. pH improves durability of paints, for protecting against harmful actions of UV, water and oxygen or any of these elements [35]. The pH values were high and close to the optimum value (pH=9) for all the emulsions considered. This higher pH is necessary to inhibit the proliferation of microorganisms, while keeping the biocides active, which gives a good and regular smell to the paint film, stabilize the additives in the emulsion [49,50]. A pH closer to 9 will inhibit the proliferation of these microorganisms, while keeping the biocides active, which gives a good and regular smell to the painted film. To ensure proper functionality of the thickener, the acidic groups in the polymer chains should be neutralized by shifting the pH value between 8 and 9.5. While, the reaction of polymerization of binder to form a cohesive film requires basic media with a pH range of 7.5–8.5. Hence, a final pH of 9 ensures an optimum thickening and maintains a stable viscosity of paint [7]. The average value of viscosity of the paints is about 120 Krebs unit (KU) at 25°C and it is in agreement with the bibliographic values for the carbonate extender (80-120 KU,) [35]. These slightly higher values of viscosity may be due to the decrease in grain size of calcite particles during the initial grinding of raw material and the paint preparation.

Density and dry extract: Density and the dry extract (ES) of formulated paint, constituted from the limestone of Merfeg Formation, are about 1.6 g/ml and 53% respectively.

Physical and mechanical properties of the painted films

Visual gloss: To obtain comparable measurement results, the reflectometers and their use at the international level have been standardized. The angle of illumination used greatly influences the value of the reflectometer. In order to be able to differentiate between very bright and dull surfaces, standardization has defined three measurement domains (Table 4). For the elaborated painted film, the value 60° < 10, considered measurement domains with matt.

Through-drying time: The through drying time of paint film taken place after 1 hour 30 minutes of exposure and no longer adheres to the finger when pressed firmly or rubs up when rubbed lightly. This relatively rapid drying is due in particular to the wetting agent action and the adequate arrangement of calcite particles in the film.

Ultrastructure of paint film: The ultrastructure of the film by SEM micrographs of a dry paint film showing a smooth surface of the film with rare pores and the white area of titanium oxide. The calcite aggregates appear to be relatively uniform in size and shape. A close-up view of the micrograph showing a rectangular calcite particle with edges and other sub-rounded. Generally, the thickness of the paint film is relatively regular no vertical stratification tendency is visible, the painted films are in general 135 µm thick (Figure 13). This uniformity results in a consistent formation of the paint film that directly affects its opacity, coverage, gloss and friction resistance [51].

Resistance to abrasion: The results show that the films tested was <5 µm thick after 200 wet friction cycles (Class 1, Table 5). This indicator is a good resistance, cleanliness and mechanical abrasion of the dry film. These properties are very suitable for interior paints application.

Performance of the carbonate calcium from the merfeg formation: The carbonates calcium from the Merfeg Formation explain a high amount of CaO as those from El Garia, Abiod Formations at the Feriana Hill and Aşıgediği Formation (Niğde Group, South Central Turkey, [7] (55.1, 55.2, 55.3 and 55.5% CaO respectively) in Table 6, which are actually used as filler in waterborne paints. The levels of harmful compounds as coloring oxides (Fe_2O_3), volatiles (Na_2O, K_2O and SO_3), MgO are very low (less than 0.5% each). The high value of CaO in the Aşıgediği Formation is due to the fact that these metamorphic carbonates are composed essentially of monomineralic calcite marble, which shifts the degree of whiteness [52-54]. The

Gloss level	Value 60°	Measure
Medium Gloss, Satin	10 To 70	Geometry 60°
Very Glossy	>70	Geometry 20°
Matt	< 10	Geomerty 85°

Table 4: The measurement domains of visual gloss.

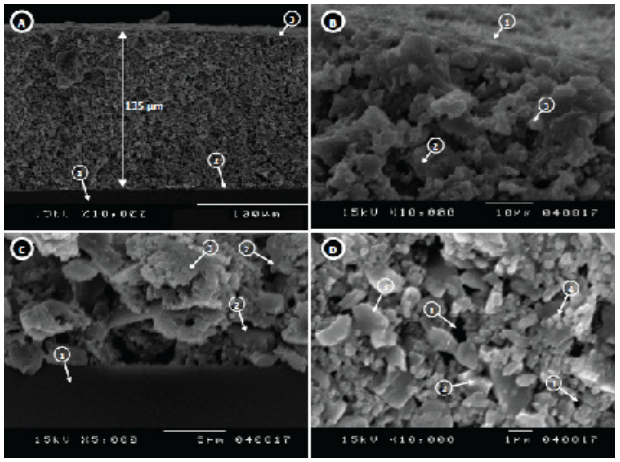

Figure 13: Scanning Electron Microscopy micrograph (SEM) images of a dry paint, showing the ultrastructure of the film. A: Section of the paint film with a relatively regular thickness (about 135 µm) and no vertical stratification trend of the film. The glass is used as substrate (1). (2) and (3) refer to lower and upper surfaces of the film respectively. B: Closer view of the upper surface of the paint film of the micrograph (A), displaying a smooth and continue layer of the polymer matrix (1) that coats calcite (2), and titania (3) particles. C: Closer view of the lower surface of the paint film of the micrograph (A). (1) substrate, (2) calcite particles and (3) polymer matrices. D: top view showing the surface of the film with rare pores of volatiles (1), calcite particles (2), polymer matrices (3), and white particles of titania (4).

Performance of the carbonate calcium from the merfeg formation: The carbonates calcium from the Merfeg Formation explain a high amount of CaO as those from El Garia, Abiod Formations at the Feriana Hill and Aşıgediği Formation (Niğde Group, South Central Turkey, [7] (55.1, 55.2, 55.3 and 55.5% CaO respectively) in Table 6, which are actually used as filler in waterborne paints. The levels of harmful compounds as coloring oxides (Fe_2O_3), volatiles (Na_2O, K_2O and SO_3), MgO are very low (less than 0.5% each). The high value of CaO in the Aşıgediği Formation is due to the fact that these metamorphic carbonates are composed essentially of monomineralic calcite marble, which shifts the degree of whiteness [52-54]. The grindability of carbonates, appreciated by Los Angeles and Micro-Deval tests (Table 6), was in general in agreement with main sources used for waterborne paints. The micro-Deval test ranked these resources as good to slightly good for the Merfeg Formation and the Barre de Ghoumrassene Member (10-18 MD), and very good for the El Garia Formations (6-10 MD), which may present slightly good grindability compared to other resources. In contrast, the Abiod Formation was categorized as a fair to poor performer (30-60 MD). The Los Angeles test, however, classes the Merfeg Formation, the El-Garia Formation and the Barre de Ghomeassene Member as hard to very hard (less than 25 LA) and classes the Abiod and the Aşıgediği Formations as soft materials (greater than 40 LA) [55]. This difference in hardness may be attributed to texture, petrographic composition and discontinuities of tested materials such as porosity, micro-fissures and stylolites. The whiteness of the raw material is in acceptable range for paint and coating applications and ranges from 83.66 to 95.58. These high values are due to the purity of carbonates and to the small mean size of calcite particle after grinding. The tested carbonates are slightly darker than those from the Abiod and Aşıgediği Formations (95.8 and 96.1 L^* respectively), which can be attributed the hydrodynamic conditions of the sedimentary environment. Indeed, lower hydrodynamic conditions promote finer sediment as clay that adsorbs coloring oxides resulting in decreasing the whiteness of limestone. The whiteness of the paint films was in general greater than 93 for all considered samples and up to 3-5% higher than raw powder, which is due to the addition of TiO_2 pigment (about 4.5%). The oil number values are in general closer to the Abiod and Aşıgediği Formations (Table 6) and ranged from 18 to 20 g/100g of calcite (17.6% in average), which is in concordance with tolerance values [35]. This difference in oil intake, which reached up to 3 g/100g of calcite between the Abiod and El Garia Formations, may be attributed to the fact that graded calcite particles are able to be compacted more than poorly graded ones, which leads to a less available space for binder [7]. Likewise, the pH values were close to the

Class of resistance	Loss in thickness
1	< 5 µm abrasion with 200 abrasion cycles
2	≥ 5 µm and < 20 µm with 200 abrasion cycles
3	≥ 20 µm and < 70 µm with 200 abrasion cycles
4	< 70 µm abrasion with 40 abrasion cycles
5	≥ 70 µm with 40 abrasion cycles

Table 5: Allocation of the resistance to wet abrasion according to standard testing (ISO 1998).

Variables		Formations/Member				
		Merfeg	Abiod [1]	Aşıgediği [1]	BDG [1]	El-Garia [2]
Raw material	Density	2.64-2.7	2.4-2.7	2.7	2.65-2.71	2.65-2.71
	Calcite (%)	98	99.38	99.1	96.4	98.1
	Texture	Packstone	Packstone	-	Packstone	Packstone
	CaO (%)	54	55.-(55.3)-55.5	55.5	53.9-(54.5)-55.2	55.24
	LOI (%)	43	43.76	43.4	42	41.9-43.2
	L*	83.66-95.58	86-(95.8)-97	96.1	86.5-97. 1	93.1
	a*	1-(1.6)-5.15	0.9-(1.4)-1.9	2.1	0.8-(2.3)-3.3	2.8
	b*	4.6-(5.9)-11.2	2.7-(5.4)-8.4	5.2	2.4-(5.6)-9.1	7.2
	Los Angeles	15-25	30-60	47 [3]	17-25	24-26
	MD	Oct-17	Oct-30	-	Oct-18	06-Oct
Emulsion	Oil number (g/100 F)	18-(17.6)-20	17	15.6-(18)-21.1	14.6-(17.4)-22.7	20
	Recipe (%)	F=58.8	F=61	F=61.5	F=61	F=45
		B=9.2	B=11.5	B=9.5	B=9.95	B=17
		P=4.5	P=5.2	P=5	P=5.7	P=5
		S+W=28.9	S+W=22.3	S+W=24	S+W=23.35	S+W=33
	Viscosity (KU)	120	95-120	80-120	91-113	-
	pH	9	9	9	9	-
Paint film	Drying time (mn)	90	180-270	180-240	180-240	90
	Thickness (µm)	135	123	106	115	80
	Abrasion	< 5 µm	< 5 µm	-	-	-
	L*	>93	>95	>97	>93	>93
	a*	0-3	0-2.5	0-2	0-3	-
	b*	0-5	0-4	0-3	0-4	-

1: Aloui et al., [7]; 2: El-Aref [54]; 3: Kahrman and Toraman [55].
BDG: Barre de Ghomrassene; F: Filler; B: Binder; P: Pigment (TiO_2); S+W: Solvent and Water. Mean values are in parenthesis

Table 6: Performance of the carbonate calcium of the Merfeg Formation compared to main Tunisian white 734 limestones and the Aşıgediği formation in South Central Turkey.

grindability of carbonates, appreciated by Los Angeles and Micro-Deval tests (Table 6), was in general in agreement with main sources used for waterborne paints. The micro-Deval test ranked these resources as good to slightly good for the Merfeg Formation and the Barre de Ghoumrassene Member (10-18 MD), and very good for the El Garia Formations (6-10 MD), which may present slightly good grindability compared to other resources. In contrast, the Abiod Formation was categorized as a fair to poor performer (30-60 MD). The Los Angeles test, however, classes the Merfeg Formation, the El-Garia Formation and the Barre de Ghomeassene Member as hard to very hard (less than 25 LA) and classes the Abiod and the Aşıgediği Formations as soft materials (greater than 40 LA) [55]. This difference in hardness may be attributed to texture, petrographic composition and discontinuities of tested materials such as porosity, micro-fissures and stylolites. The whiteness of the raw material is in acceptable range for paint and coating applications and ranges from 83.66 to 95.58. These high values are due to the purity of carbonates and to the small mean size of calcite particle after grinding. The tested carbonates are slightly darker than those from the Abiod and Aşıgediği Formations (95.8 and 96.1 L^* respectively), which can be attributed the hydrodynamic conditions of the sedimentary environment. Indeed, lower hydrodynamic conditions promote finer sediment as clay that adsorbs coloring oxides resulting in decreasing the whiteness of limestone. The whiteness of the paint films was in general greater than 93 for all considered samples and up to 3-5% higher than raw powder, which is due to the addition of TiO_2 pigment (about 4.5%). The oil number values are in general closer to the Abiod and Aşıgediği Formations (Table 6) and ranged from 18 to 20 g/100g of calcite (17.6% in average), which is in concordance with tolerance values [35]. This difference in oil intake, which reached up to 3 g/100g of calcite between the Abiod and El Garia Formations, may be attributed to the fact that graded calcite particles are able to be compacted more than poorly graded ones, which leads to a less available space for binder [7]. Likewise, the pH values were close to the optimal value (9 pH unit) for all the emulsions considered and high enough to prevent the proliferation of alga and microorganisms on the paint film with time [35].

Conclusion

As shown above, the following salient findings were highlighted:

1. The limestones of the Merfeg formation in Central Tunisia are marked by a high to very high degree of purity, with a CaO content ranging between 94.5% to 98.6%. The others oxides are extremely low in particular the MgO (less than 0.1% on average), Al_2O_3, Fe_2O_3, K_2O and Na_2O (less than 1% each).
2. The Fe_2O_3 constitute one of the major coloring oxides that may alter the whiteness of the raw material. This oxide is low (less than 0.5%) and is detectible near fractures, karst corrosion, bedding planes, tectonic discontinuity and even through the rock inform of small concretions of iron.
3. The limestone of the Merfeg formation has a bright white color ($L^* \geq 83.66$ to 95.58) and exhibits a minor trend to yellow–red ($a^*=1.6$ and $b^*=5.9$). The brightness reading of raw material (L^*) increases as calcite and quartz increase from bottom to top of layers. However, it decreases dramatically near fault zones and karstic cavities, where aggregates explain darker and reddish to pinkish appearance.
4. The carbonate of the study area has a low oil intake (18 g/100 calcites), very low acid insoluble residue (less than 0.1%), good pH buffering (close to 9), easy dispersion with adequate viscosity (120 KU) and improved rheological properties.
5. The results of physical and mechanical tests applied to the elaborated films based on limestone from Merfeg Formation of the study area using a standard recipe meet, show 1 hour 30 minutes for the through drying time, with the thickness of painted films is 135 µm and good abrasion resistance of the dry film and matt visual gloss, and high luminescence reading not less than $L^*=93$ (suggested by the norm).
6. For all considered parameters of quality such as color, opacity and mechanical behavior of the paint film, the performances of end-product based on the limestones from the Merfeg formation are analogous to the Tunisian calcium carbonates resources in particular those of the Abiod formation, the Barre de Ghomrassene member and the El-Garia formation. But they are slightly less light than those Turkish carbonates of Aşıgediği formation.

References

1. Boynton RS (1980) Chemistry and technology of lime and limestone. John Wiley & Sons 4: 380-486.
2. Burollet PF (1956) Contribution to the stratigraphic study of Central Tunisia. Ann. Mines Geol 18: 350.
3. Bousson G (1967) The Mesozoic Saharan. 1st part: The Tunisian Far South [The Mesozoic Saharan. 1st part: The Tunisian Far South] (1st edn). National Center for Scientific Research, Paris. p: 194.
4. Bouaziz S, Donze P, Ghanmi M, Zarbout M (1989) The predominantly continental series (Oxfordian to Cenomanian) of the cliff of Dahar (South-Tunisian); its evolution from Tebaga of Medenine to the Tripolitan border. Mediterranean Geology 16: 67-76.
5. Chaabani F (1995) Dynamics of the eastern part of the Gafsa basin in the Cretaceous and Paleogene: Mineralogical and geochemical study of the Eocene phosphate series, southern Tunisia Tunis: Univrsity of Tunis.
6. Enay R, El Asmi K, Soussi M, Mangold C, Hantzpergue P (2002) An Arabic Pachyerymnoceras in the Upper Callovian of Dahar (southern Tunisia), new element of dating of the Ghomrassene member (Tataouine formation); correlations with Saudi Arabia and the Middle East. C R Geosci 334: 1157-1167.
7. Aloui T, Jabli I, Hermassi A, Chaabani F (2018) Ground Calcium Carbonate (GCC) from the Barre de Ghomrassene, in Southeast Tunisia: A suitable raw material for paint industry. Arab J Geosci. 11: 1-18.
8. Abdeljaoued S, Zargouni F (1985) Evidence of intra-cretaceous tectonics in the eastern end of the chain of Chotts. In: Proceedings of the First National Congress of Earth Sciences pp: 285-290.
9. Boukadi N (1985) Evolution géodynamique et cinématique de la zone d'interférence de l'Axe Nord-Sud et de la chaine de Gafsa (Maknassy-Mezzouna et Jebel Bouhedma) [Geodynamic and kinematic evolution of the zone of interference of the North-South Axis and the Gafsa chain (Maknassy-Mezzouna and Jebel Bouhedma)] [dissertation]. Paris: Louis Pasteur University.
10. Fournie D (1975) Sequential analysis and sedimentology of the Ypresian of Tunisia. Bull Cent Rech Explor Prod Elf-Aquitaine 9: 27-75.
11. Aloui T, Chaabani F (2007) Influence of fractures and karstification on the development of a quarry at Jebel Feriana, Tunisia. Bulletin of Engineering Geology and the Environment. 66: 345-351.
12. Ben Ferjani, F, Burollet PF, Mejri F (1990) Petroleum geology of Tunisia. Report, Tunisian Company of Petroleum Activities, Tunis pp: 194.
13. Jarvis I, Mabrouk A, Moody RTJ, De Cabrera S (2002) Late Cretaceous (Campanian) carbon isotope events, sea-level change and correlation of the Tethyan and Boreal realms. Palaeogeogr Palaeoclimatol Palaeoecol. 188: 215-248.
14. Sdiri A, Higashi T, Hatta T, Jamoussi F, Tase N (2010) Mineralogical and

spectroscopic characterization, and potential environmental use of limestone from the Abiod formation, Tunisia. Environ Earth Sci. 61: 1275-1287.

15. Aloui T, Chaabani F (2008) Maastritchian limestones of Feriana Mountain used in white cement production (Central West Tunisia). J Am Ceram Soc 91: 3704-3713.
16. Aloui T, Rhimi L, Jabli I, Hermassi A, Chaabani F (2017) Use of Late-Barremian sands from Central Tunisia in white cement clinker. Arab J Geosci 10: 1-18.
17. Sdiri A, Bouazir S (2014) Re-evaluation of several heavy metal's removal by natural limestones. Front. Chem. Sci. Eng. 2014, 8: 418–432.
18. Khessibi M (1978) Geological survey of Maknassy-Mezzouna and Jebel Kebar (Central Tunisia) [Geological survey of Maknassy-Mezzouna and Jebel Kebar (Central Tunisia)] [dissertation]. University of Lyon, Lyon.
19. Negra MH (1984) Paléoenvironnement et diagenèse des facies récifaux _a rudists du Jebel Kébar, Central Tunisie. Doctoral thesis, Université de Paris, Orsay, France. p: 290.
20. Rabet A (1986) Stratigraphie, sedimentation et diagenese carbonatée des series du Crétacé inférieur de Tunisie centrale [Stratigraphy, sedimentation and carbonate diagenesis of the Lower Cretaceous séries of central Tunisia] [Dissertation]. University of Paris-Sud, Paris.
21. Cox F, McC, Bridge D, Hull JH (1977) Procedures for the assessment of limestone resources. Miner Assess Rep Inst Geol Sci pp: 30
22. Broad R, Power G, Sonego A (1993) Extender pigments. In: Oil and Colour Chemists' Association (ed), Surface coatings. Springer pp 514-529.
23. Dillon CE, Lagalante AF, Wolbers RC (2014) Acrylic emulsion paint films: the effect of solution pH, conductivity, and ionic strength on film swelling and surfactant removal. Studies in Conservation. 59: 52-62.
24. Negra MH (1994) Upper cretaceous basin platform deposits in North-Central Tunisia. Sedimentation and diagenesis of upper cretaceous series (Abiod formation and associated facies). Stratigraphy, sedimentation, diagenesis and petroleum interest. PhD Es-Sciences thesis, University of Tunis. p: 548.
25. Negra MH, Purser BH, M'Rabet A (1995) Sedimentation, diagenesis and syntectonic erosion of Upper Cretaceous rudist mounds in central Tunisia. Spécial Publication of the International Association of Sedimentologists 23: 401-419.
26. Kadri A, Essid EM, Merzeraud G (2015) Limit emerged boundaries of "Kasserine Island" changed during the Upper Cretaceous-Eocene (Central Tunisia). Journal of African Earth Sciences 111: 244-257.
27. Negra MH (1984) Nature and origin of rudist "reefs" of Jebel el Kébar, Central Tunisia. 5th I.A.S.Reg. Meeting. Marseille p: 318-319.
28. Negra MH (1984) Paleoenvironment and diagenesis of rudist reef facies in Jebel el Kébar, Central Tunisia. Paris: University of Paris, Orsay.
29. Ouali J, Martinez C, Khessibi M (1986) Caracteres de la tectonique cretacee en distension au Jebel Kebar (Tunisie Centrale): ses conséquences. Géodynamique 1: 3-18.
30. Jaballah J, Negra MH (2016) Stratigraphic and sedimentary characters of Late Cretaceous formations outcropping in central and southern Tunisia, Tethyan southern margin. J Afr Earth Sci 124: 289-310.
31. Ruste J (1978) X-ray spectroscopy (X-ray spectroscopy). In: Les éditions de physique (eds.), Microanalyse–Microscopie Electronique A Balayage (Microanalysis–electron scanning microscopy). France. pp: 219-272.
32. Blanco-Varela MT, Palomo A, Puertas F, Vazquez T (1997) CaF_2 and $CaSO_4$ in white cement clinker production. Advances in Cement Research 9: 105-113.
33. Commission Internationale de l'Eclairage (CIE) (1986) Standard on colorimetric observers. CIE S002, New York.
34. Köhler K, Simmendinger P, Roelle W, Scholz W, Valet A, et al. (2000) Paints and coatings, 4. Pigments, extenders, and additives. Ullmann's encyclopedia of industrial chemistry pp: 22.
35. ASTM (2014) Standard test methods for specific gravity of soil solids by water pycnometer. Designation: D854–14. American Society for Testing and Materials, USA.
36. ASTM (2017) Standard test method for resistance of coarse aggregate to degradation by abrasion in the micro-deval apparatus. Designation: D6928–17. American Society for Testing and Materials, USA.
37. ASTM (2016) Standard test method for oil absorption of pigments by spatula rub-out. Designation: D281–12. American Society for Testing and Materials, USA.
38. Grandou P, Pastour P (1966) Peintures et Vernis - Les constituants - Liants, solvants, plastifiants, pigments, colorants, charges, adjuvants Hermann [Paints and Varnishes - Constituents - Binders, Solvents, Plasticizers, Pigments, Dyes, Fillers, Adjuvants Hermann] pp: 944.
39. Karakaş F, Celik MS (2012) Effect of quantity and size distribution of calcite filler on the quality of water borne paints. Prog Org Coat 74: 555-563.
40. Cremer M (1985) TiO_2 white pigments with special reference to ZnS pigments "IM" Pigments and Extenders. Supplément pp:16-21.
41. Koleske JV (2012) Paint and coating testing manual (15th edn) of the Gardner-Sward handbook. ASTM International.
42. ASTM (2014) Standard test method for consistency of paints measuring Krebs Unit (KU) viscosity using a Stormer-type viscometer. Designation: D562–10. American Society for Testing and Materials.
43. International Organization for Standardization ISO 3251. Paints and varnishes - Determination of the dry extract of paints, varnishes and binders for paints and varnishes margin.
44. ASTM (2008) Standard test method for specular gloss. Designation: American Society for Testing and Materials pp: 523-89.
45. ASTM (2013) Standard test methods for measurement of wet film thickness of organic coatings. Designation: D1212–91. American Society for Testing and Materials USA.
46. Gooch JW (2011) Encyclopedic Dictionary of Polymers (2nd edn). Springer pp: 520.
47. International Organization for Standardization. ISO 1998 (2006) Paints and varnishes - Determination of wet rub resistance and cleaning ability of coatings.
48. Lindner W (2001) New developments for in-can preservation of water-based paints and printing inks. Surface Coatings International Part B: Coatings Transactions 84: 141-146.
49. Dillon CE, Lagalante AF, Wolbers RC (2014) Acrylic emulsion paint films: the effect of solution pH, conductivity, and ionic strength on film swelling and surfactant removal. Studies in Conservation 59: 52-62.
50. Karakas F, Hassas BV, Celik MS (2015) Effect of precipitated calcium carbonate additions on waterborne paints at different pigment volume concentrations. Progress in Organic Coatings 83: 64-70.
51. Whitney DL, Dilek Y (1998) Metamorphism during crustal thickening and extension in central Anatolia: the Nigde metamorphic core complex. J Petrol 39: 1385-1403.
52. Whitney DL, Teyssier C, Fayon AK, Hamilton MA, Heizler M (2003) Tectonic controls on metamorphism, partial melting, and intrusion: timing of regional metamorphism and magmatism of the Nigde Massif, Turkey. Tectonophysics. 376: 37-60.
53. Pohl WL (2011) Principles and practice metals, minerals, coal and hydrocarbons-introduction to formation and sustainable exploitation of mineral deposits. Wiley-Blackwell pp: 699.
54. El-Aref M (2012) Possibility of using calcium carbonates from Jebel Jebil's EL Garia formation in the manufacture of paint [Master's thesis]. University of Tunis El-Manar, Tunis.
55. Kahrman S, Toraman OY (2008) Predicting Los Angeles abrasion loss of rock aggregates from crushability index. B Mater Sci 31: 173-177.